A New Analysis of Beam-Waveguide Antennas Considering the Presence of the Enclosure

A. G. Cha
Ground Antenna and Facilities Engineering Section

Beam-waveguide (BWG) antennas provide multiple frequency band operations and other operational benefits for large ground-station antennas. Present design practices use diffraction analyses that ignore the presence of the BWG enclosure and may be inaccurate at lower frequency bands for ground-station antennas operating over multiple frequency bands. This article introduces a new analysis approach that considers the presence of the BWG enclosure. Results based on the new analysis have revealed new understandings of the performance degradation mechanisms in a BWG antenna and have provided direction for potential design improvements.

I. Introduction

Beam-waveguide (BWG) technology offers wide frequency-band coverages, improved gain/temperature (G/T) performance for ultra-low-noise ground antennas by providing a more stable operating environment for masers, advantages in maintenance and operations, and reduced life-cycle cost for ground-station antennas. For these reasons, there has been a trend towards adopting the BWG design in new ground-station antenna projects. Examples are the Japanese 45-m and 64-m antennas at Nobeyama and Usuda, and various 30-m class Intelsat and Comsat ground antennas. Additionally, the Deep Space Network (DSN) is building a 34-m BWG antenna at Goldstone, California.

The BWG feed operating principle is based on geometric optics (GO). By using a pair of properly shaped and positioned mirrors, the radiation pattern of a feedhorn can be reproduced at a point in space that is some distance away from the physical location of the feedhorn. For finite-size BWG systems and at finite frequencies, some loss and some pattern distortions are experienced. At present, such effects are predicted from diffraction analysis developed for mirrors in open space. Common analysis techniques are Gaussian mode analysis and physical optics (PO) analysis. In actuality, the BWG mirrors are enclosed by metal walls for safety when transmitting, and for sensitivity (noise temperature) and protection against radio frequency interference (RFI) when receiving. The absence of the metal wall in the current analysis models leads to an error whose magnitude is not well understood, especially at lower frequencies when the wall diameter is 20 wavelengths or less. In practice, this means one is forced to make decisions about, for example, building a 6-ft- or 8-ft-diameter BWG system based on weak assumptions. Such decisions often have major impacts on antenna microwave/structural performances and project cost tradeoffs.

This article presents a new analysis of BWG antennas which considers the presence of the wall. This analysis is based on

replacing the free-space Green's function used in PO analysis with the dyadic Green's function for a cylindrical waveguide, satisfying the boundary condition at the metallic BWG wall. The results from this analysis have revealed some new understandings of the performance degradation mechanisms in a BWG antenna and have pointed to potentially significant design improvements. Some of these ideas are discussed here. Full realization of all benefits from BWG wall analysis and design concepts will take some time. It is hoped that the discussions in this article will induce further innovative ideas and designs.

II. The Optics of BWG Systems

Figures 1(a) and 1(b) show the microwave optics of BWG systems. A basic cell consists of a pair of curved mirrors (reflectors). In practice, a pair of flat mirrors is often added to form a four-mirror system. However, the BWG characteristics are largely determined by the pair of curved mirrors. The conditions for distortionless transmission of feedhorn patterns based on GO are discussed in [1]. It is shown that a paraboloid pair oriented as shown in Fig. 1(a) is one choice that meets the Mizusawa condition. This case is used here to discuss the diffraction effects.

The Mizusawa condition guarantees distortionless transmission of the feedhorn pattern from focus F1 to focus F2 at infinite frequency where GO is valid. The only loss is at the first mirror as it does not collect all the GO rays. In practice, BWG antenna designs must consider diffraction effects which cause further degradations as shown in Fig. 1(b). Figure 1(b) illustrates how the diffraction effects are presently modeled. Mirror 1 is illuminated by the feedhorn and radiates into the whole space. Assuming mirror 2 is in the near-field zone of mirror 1, one can visualize mirror 2 intercepting the bulk of the rays bounced off mirror 1, but there is a small amount of energy loss due to the divergence of the beam of rays. In addition, it can also be expected that the rays reflected from mirror 2 will now not be focused to a single point F2. This implies that the image pattern at F2 compared to the real feedhorn pattern at F1 will have amplitude and phase distortions. If the real feedhorn pattern at F1 is the ideal pattern needed to illuminate a reflector antenna, then the distorted pattern at F2 gives rise to further performance degradations in addition to the spillover loss at each mirror.

Such mechanisms of performance degradation are predicted from present analytical techniques, including Gaussian mode analysis [2], physical optics [3], and geometrical theory of diffraction (GTD). It is generally accepted that these techniques yield good results under the very near-field approximation.

$$L \leq C\left(\frac{D^2}{\lambda}\right) \tag{1}$$

where L is the distance between mirrors 1 and 2, D is the mirror diameter, λ is the wavelength, and C is a constant generally taken as between 0.1 and 0.2 [3]. None of the above analyses recognizes the presence of the wall and thus they are likely to lead to errors in BWG antenna performance analysis when the condition in Eq. (1) is not met. The following introduces a new analytical approach that recognizes the wall presence. The new analysis is theoretically more satisfactory and should in time lead to significantly better analysis and design of BWG antennas.

III. New BWG Antenna Analysis That Considers the Wall Presence

The new BWG wall analysis presented in this article is conceptually similar to the PO analysis used in reflector antenna analysis; Fig. 2 shows this analogy. The PO analysis and the BWG wall analysis can each be conceptualized as a superpositioning process whereby the radiation field of a current distribution is found by integrating the radiation field of point sources. Assuming a time dependence $e^{j\omega t}$, the PO far field is written as

$$\bar{E}(\bar{R}) = I_\theta\,\hat{\theta} + I_\phi\,\hat{\phi} \tag{2}$$

where

$$\bar{I} = -j\omega\mu\int \bar{K}(\bar{R}')\,g(\bar{R},\bar{R}')\,ds' \tag{3}$$

and

$$g(R, R') = \frac{e^{-jk|\bar{R}-\bar{R}'|}}{4\pi|\bar{R}-\bar{R}'|} \tag{4}$$

In Eqs. (2), (3), and (4), ω is the angular frequency, μ is the permeability, $\bar{R}$ is the position vector of the observer, $\bar{R}'$ is the position vector of a point source, and $g(\bar{R}, \bar{R}')$ is the free-space Green's function. The integration is over the surface current as determined from the PO approximation, i.e.,

$$\bar{K}(\bar{R}') = 2\hat{n} \times \bar{H}^{inc}(\bar{R}')$$

where $\hat{n}$ is the unit normal vector and $\bar{H}^{inc}$ is the incident magnetic field. For BWG analysis, the approach in this article is based on a very elegant dyadic Green's function formulation

discussed in [4]. For the one-mirror BWG system, the field scattered by the BWG mirror in the waveguide can be written as

$$\bar{E} = -j\omega\mu \int \bar{\bar{G}}_1(\bar{R}, \bar{R}')\, \bar{K}\, ds' \tag{5}$$

where $\bar{\bar{G}}_1(R, R')$ is the dyadic Green's function that satisfies Maxwell's equations and the boundary conditions of the BWG metal wall, i.e., no field exists outside the BWG wall. For a cylindrical waveguide, the dyadic Green's function has been derived and is given in Eq. (15) of [4] as

$$\begin{aligned}\bar{\bar{G}}_1(\bar{R}, \bar{R}') = {} & \frac{-j}{4\pi} \sum_{1=1}^{2} \sum_{n=0}^{\infty} \sum_{m=1}^{\infty} (2 - \delta_o) \\ & \times \left[\frac{1}{\mu^2 I_\mu k_\mu} \bar{M}_{\substack{e \\ o}\, nm}(k_\mu) \bar{M}'_{\substack{e \\ o}\, nm}(-k_\mu) \right. \\ & \left. + \frac{1}{\lambda^2 I_\lambda k_\lambda} \bar{N}_{\substack{e \\ o}\, nm}(k_\lambda) \bar{N}'_{\substack{e \\ o}\, nm}(-k_\lambda) \right] \\ & - \frac{1}{k^2} zz\, \delta(\bar{R} - \bar{R}'), \qquad z > 0 \end{aligned} \tag{6}$$

where $\delta(\bar{R} - \bar{R}')$ is the Dirac delta function, δ_o is the Kronecker delta, $\delta_o = 0$ if $n \neq 0$ and $\delta_o = 1$ if $n = 0$, and the 1-summation is over even and odd modes. Note that in Eq. (6), μ, I_μ, k_μ, λ, I_λ, and k_λ are understood to have double indices m and n.

$$\bar{M}_{\substack{e \\ o}\, nm}(h) = \left[\mp \frac{nJ_n(\mu r)}{r} \begin{matrix} \sin \\ \cos \end{matrix} n\phi \hat{r} - \frac{\partial J_n(\mu r)}{\partial r} \begin{matrix} \cos \\ \sin \end{matrix} n\phi \hat{\phi} \right] e^{-jhz} \tag{7}$$

$$\bar{N}_{\substack{e \\ o}\, nm}(h) = \frac{1}{k} \left[-jh \frac{\partial J_n(\lambda r)}{\partial r} \begin{matrix} \cos \\ \sin \end{matrix} n\phi \hat{r} \right. \\ \left. \pm \frac{jhn}{r} J_n(\lambda r) \begin{matrix} \sin \\ \cos \end{matrix} n\phi \hat{\phi} + \lambda^2 J_n(\lambda r) \begin{matrix} \cos \\ \sin \end{matrix} n\phi \hat{z} \right] e^{-jhz} \tag{8}$$

$$I_\lambda = \int_o^a J_n^2(\lambda r)\, r\, dr = \frac{a^2}{2\lambda^2} \left[\frac{\partial J_n(\lambda r)}{\partial r} \right]^2_{r=a} \tag{9}$$

$$I_\mu = \int_o^a J_n^2(\mu r)\, r\, dr = \frac{a^2}{2\mu^2} \left(\mu^2 - \frac{n^2}{a^2} \right) J_n^2(\mu a) \tag{10}$$

In Eqs. (9) and (10), a is the radius of the waveguide, k is the free-space wave number, and J_n is the Bessel function of the first kind.

To satisfy the radiation condition, when k_μ and k_λ are real,

$$k_\mu = |(k^2 - \mu^2)^{1/2}|$$

$$k_\lambda = |(k^2 - \lambda^2)^{1/2}|$$

When they are imaginary ($k^2 < \mu^2, k^2 < \lambda^2$),

$$k_\mu = (-j)\,|(\mu^2 - k^2)^{1/2}|$$

$$k_\lambda = (-j)\,|(\lambda^2 - k^2)^{1/2}|$$

$$\mu = \mu_{nm} = \frac{q_{nm}}{a} \tag{11}$$

$$\lambda = \lambda_{nm} = \frac{p_{nm}}{a} \tag{12}$$

In Eqs. (11) and (12), q_{nm} and p_{nm} are the mth root of $J_n(x)$ and $J_n'(x)$.

$$J_n(p_{nm}) = 0$$

$$\left. \frac{dJ_n(x)}{dx} \right|_{x=q_{nm}} = 0$$

$$k = \frac{2\pi}{\lambda_0}$$

where λ_0 is the free-space wavelength.

Note that M and N in Eqs. (7) and (8) represent TE and TM waves propagating in the $+z$ direction. Individually, each mode satisfies Maxwell's equation, the boundary conditions at the wall, and the "radiation condition" as $z \to \infty$. It is clear that Eq. (5) is conceptually the equivalent of PO in the beam-waveguide world. The difference is in Green's functions, which must meet different boundary conditions, including the radiation condition.

IV. Numerical Results and Assessment

The results of the wall analysis of a 34-m antenna under construction (designated DSS-13 in the DSN) are shown in Fig. 3. The projected mirror diameter is approximately 2.4 m, or approximately 19 wavelengths at the analysis frequency of 2.295 GHz. These initial results revealed some exciting potential for BWG antenna design improvement. A very important finding is that there are only a few significant modes propagating between the two curved mirrors. This is despite the facts that the waveguide diameter is 19 wavelengths, and that a large number of modes are theoretically above their cutoff frequencies. As shown in Fig. 3, the electromagnetic (EM) field scattered from mirror 1 consists of mainly TE_{11} and TM_{11} modes. This is not surprising, as the incident field is assumed to be from a horn with a symmetric radiation pattern, similar to that of a corrugated horn. By normalizing the mode power to the TE_{11} mode, the third and fourth significant modes TE_{21} and TM_{21} are already about 30 dB down in power.

Given that hundreds of modes may propagate, this result must be viewed with some caution. It is encouraging that the results described above are in qualitative agreement with some results in [2]. By expanding the reflected field from a curved mirror in Gaussian modes, the field can be represented approximately by just two Gaussian modes, TEM_{00} and TEM_{01}. Note that the field line of the TEM_{00} Gaussian mode bears a striking similarity to that of the aperture field of a dual-mode (TE_{11} and TM_{11}) horn, with the two modes in appropriate amplitude and phase relationships. Furthermore, the TEM_{01} Gaussian mode field lines are similar to the TE_{21} cylindrical waveguide mode. These observations are shown in Fig. 4. Thus the results in [2] are in qualitative agreement with the present analysis with regard to the scattered field from mirror 1 in the immediate neighborhood of mirror 1.

The major difference between a Gaussian mode analysis and the present analysis is that Gaussian modes and cylindrical waveguide modes propagate with distinctly different characteristics between mirrors 1 and 2. One significant difference is that the dominant Gaussian TEM_{00} is seen to be more like two cylindrical waveguide modes. For large mirror separations, there is phase slippage between the two cylindrical waveguide modes not predicted by the TEM_{00} mode. Clearly, the Gaussian mode analysis is appropriate for BWG systems not enclosed by metal walls. When it is applied to an enclosed BWG system, it is a good approximation only while Eq. (1) is valid. The present analysis is valid when the BWG system is enclosed in metal walls and does not appear to be bound by Eq. (1), at least in principle.

A discussion follows of the mechanisms that cause performance degradation in an enclosed BWG system. These are

(1) mode generation

(2) mode dispersion

(3) spillover loss at each mirror

(4) multiple scattering between mirrors

(5) dissipative loss in the wall

Assume that an HE_{11} mode horn or equivalently a dual TE_{11} and TM_{11} mode horn illuminates mirror 1. Each curved mirror may be viewed as a mode generator whose scattered field contains unwanted higher-order modes in the sense that at the output end of the BWG system, only the TE_{11} and TM_{11} modes in the correct complex ratio are desired. It appears that mode dispersion is a limiting factor, i.e., propagation with different phase velocities in the BWG causes the various modes to appear in wrong phases at the output of the BWG system. Undoubtedly, the present analysis provides the correct basis for calculating mode dispersion in an enclosed system compared to existing approaches such as Gaussian mode, PO, GTD, or others. Mechanisms (4) and (5) listed above have not been modeled, although a description of dissipative loss that ignores mechanisms (3) and (4) is within reach in the context of the present analysis. Ignoring the multiple-scattering mechanism nonetheless yields good results, as it appears to be much less important than mode generation and dispersion effects in a first-order analysis.

In terms of design improvements, the greater accuracy of the wall analysis model at lower frequencies should lead to more cost-effective designs of BWG antennas. Specifically, the diameter of the BWG tube is determined by low-frequency performance requirements. A less accurate analysis tends to lead to an unnecessarily large BWG tube, which raises antenna construction costs. Since a section of the BWG tube runs parallel to the antenna elevation axis, a larger tube requires the reflector and its backup structure to be raised higher, increasing the moment of the reflector and backup structure about the elevation axis. This reduces the antenna's pointing performance in wind, which must be compensated for by a

heavier, more expensive design. The alternative is that a reduced antenna wind pointing performance must be accepted. In addition, the analytical results showing that there are only a few significant modes likely between mirrors 1 and 2 suggest some further improvements to the BWG antenna and feed design. Since most of the power is in the TE_{11} and TM_{11} modes and the differential propagating phase of the modes can be computed, it appears possible to design a dual-mode or multimode horn to compensate for the mode generation and mode dispersion effects discussed above.

Acknowledgments

The author wishes to acknowledge Mr. R. C. Clauss of JPL for many stimulating discussions pertaining to the BWG wall effects and Mr. M. J. Gans of AT&T Bell Laboratories for allowing the use of Fig. 4 in this paper, which is from [2]. Also, J. Schredder has helped tremendously with software development based on the wall analysis.

References

[1] M. Mizusawa and T. Kitsuregawa, "A Beam Waveguide Feed Having a Symmetric Beam for Cassegrainian Antennas," *IEEE Trans. Antennas and Propagation*, vol. AP-21, pp. 884-886, November 1973.

[2] M. J. Gans, "Cross Polarization in Reflector Type Beam Waveguides and Antennas," *The Bell System Technical Journal*, pp. 289-316, March 1976.

[3] K. K. Chan, "Some Aspects of Beam Waveguide Design," *IEE Proc.*, vol. 129, pt. H, no. 4, pp. 203-210, August 1982.

[4] C. T. Tai, *Dyadic Green's Functions in Electromagnetic Theory*, Scranton, Pennsylvania: Intext Educational Publishers, 1971.

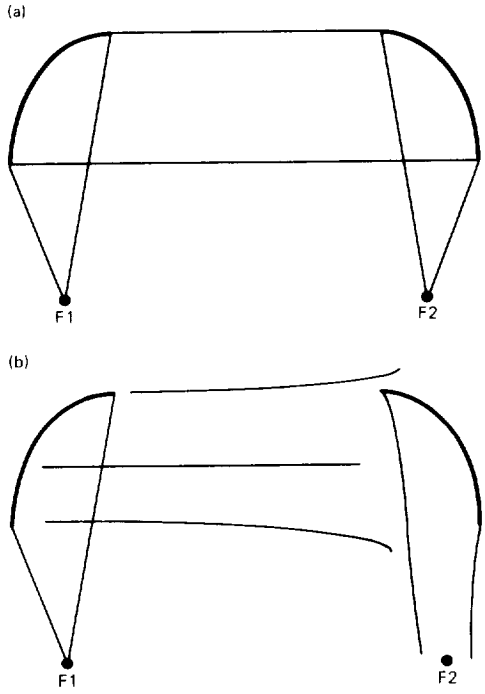

Fig. 1. Optics of BWG systems: (a) geometric optics approximation; (b) diffraction analysis with mirrors in open space.

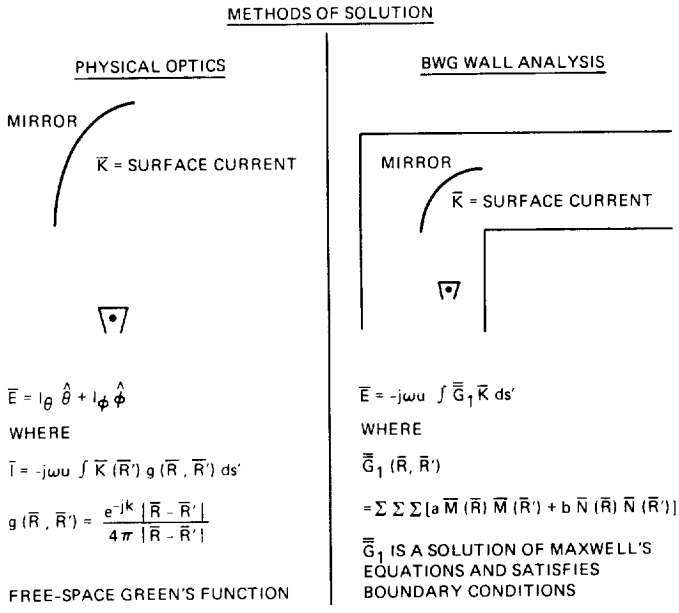

Fig. 2. Enclosed BWG system analysis approaches.

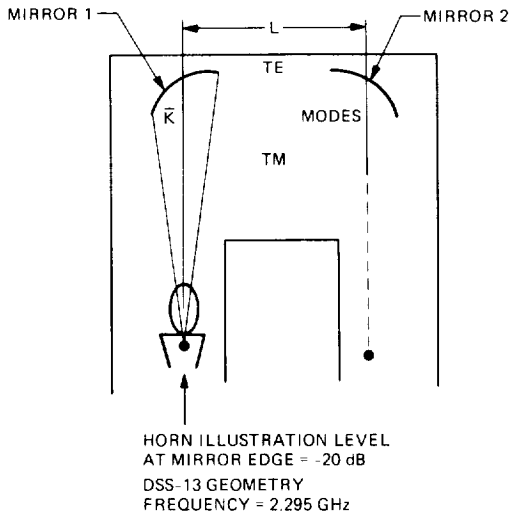

MODE POWER CONTENTS

MODE	MODE COEFFICIENTS	
TE_{11} EVEN	0.24 + j 0.88	0 dB
TM_{11} ODD	0.25 - j 0.07	-10.9 dB
TE_{21} EVEN	-0.01 - j 0.03	-29.6 dB
TM_{21} ODD	-0.02 - j 0.0	-33.2 dB

Fig. 3. Results of one-mirror BWG system wall analysis.

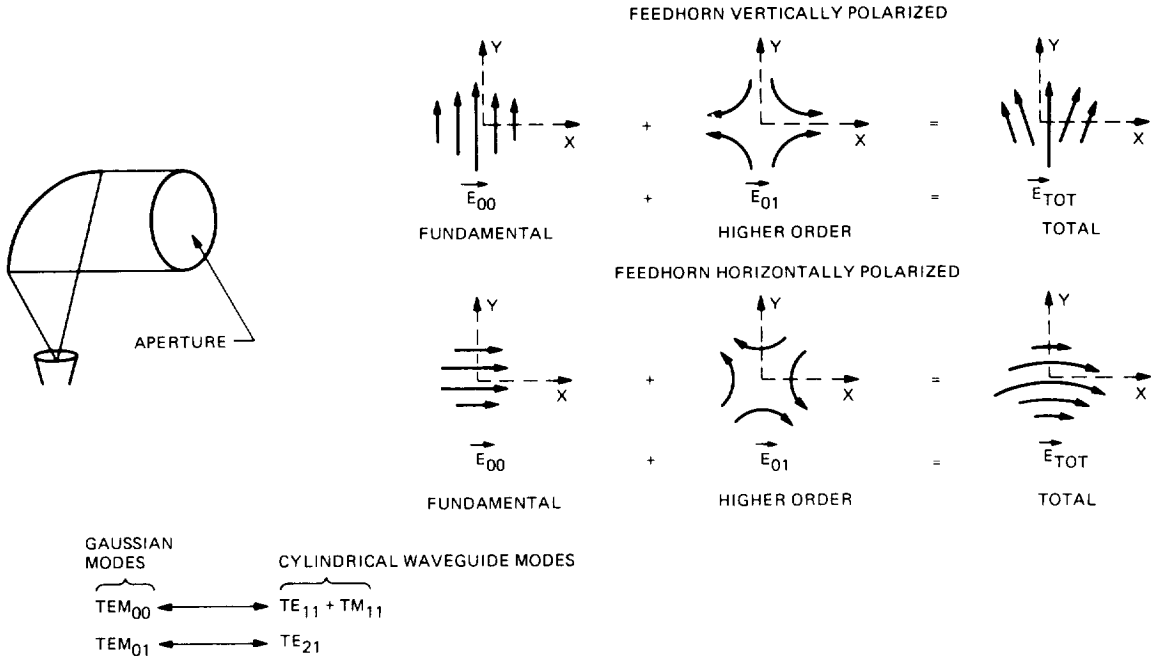

Fig. 4. Two-mode decomposition of aperture field.